Nano Research
DOI 10.1007/s12274-013-0304-z
Research Article
ISSN 1998-0124
CN 11-5974/O4

Raman scattering study of the phonon dispersion in twisted bilayer graphene

Jessica Campos-Delgado[1] (✉), Luiz G. Cançado[2], Carlos A. Achete[3], Ado Jorio[2], and Jean-Pierre Raskin[1]

[1] *Institute of Information and Communication Technologies, Electronics and Applied Mathematics (ICTEAM), Université catholique de Louvain, Louvain-la-Neuve, 1348, Belgium*
[2] *Departamento de Física, Universidade Federal de Minas Gerais, Belo Horizonte, MG, 30123-970, Brazil*
[3] *Divisão de Metrologia de Materiais, Instituto Nacional de Metrologia, Qualidade e Tecnologia (INMETRO), Xerém, RJ, 25250-020, Brazil*

Received: 28 January 2013
Revised: 7 March 2013
Accepted: 10 March 2013

KEYWORDS
twisted bilayer graphene, Raman spectroscopy, phonon branches

ABSTRACT

Bilayer graphene with a twist angle θ between the layers generates a superlattice structure known as a Moiré pattern. This superlattice provides a θ-dependent $\boldsymbol{q}$ wavevector that activates phonons in the interior of the Brillouin zone. Here we show that this superlattice-induced Raman scattering can be used to probe the phonon dispersion in twisted bilayer graphene (tBLG). The effect reported here is different from the widely studied double-resonance in graphene-related materials in many aspects, and despite the absence of stacking order in tBLG, layer breathing vibrations (namely ZO′ phonons) are observed.

1 Introduction

The double-resonance (DR) Raman scattering mechanism has been extensively explored in graphene-based materials [1–3]. Having been studied in graphite [4–8], graphite whiskers [9], carbon nanotubes [10–13], graphene [14, 15], nanographite and amorphous carbons [16, 17], the DR Raman is a striking effect that allows one to probe the interior of the phonon dispersion relation using visible light by changing the excitation laser energy. It was introduced by Thomsen and Reich [4] to explain the observation of a defect-induced D band in graphitic materials, the one-phonon Raman scattering process being always constrained to the existence of defects to break the $\boldsymbol{q} \cong 0$ momentum selection rule. Furthermore, the DR mechanism selects the modulus of the phonon wavevectors $|\boldsymbol{q}|$, and the observed peaks give an average of the phonon frequencies observed around the high symmetry Γ and K points in the graphene Brillouin zone [5], pounded by the electron–phonon interaction which is wavevector direction dependent [15].

Bilayer graphene with a mismatch angle θ between the layers, named twisted bilayer graphene (tBLG), generates a modulation which activates one-phonon Raman processes without requiring defects [18–20]. This effect has been observed recently by different

Address correspondence to jessica.campos@uclouvain.be

groups [18–23], and here we provide a unifying picture that accounts for all the Raman peaks observed in tBLG, showing that the superlattice-induced Raman process allows us to probe the phonon dispersion of tBLG. Different from previously studied DR in graphene-based systems, in tBLG the phonon dispersion can be probed without changing the excitation laser energy, without the presence of defects or higher-order processes, and the process is q-direction selective.

2 Results and discussion

Our sample is composed of a monolayer film where bilayer and multilayer islands can be observed. These islands sitting on monolayer graphene have in general a multi-lobe star morphology; the lobes constituting the second layer and, in the center, three or more stacked layers can be identified by optical contrast when using an optical microscope.

Recently, it has been proven that the electronic properties of twisted bilayer graphene combined with its reflection on a 100 nm-thick SiO_2/Si substrate make twisted bilayer graphene ($9° < \theta < 16°$) visible through the appearance of blue, yellow or pink/red colorations [24, 25]. We have transferred our samples to Si/SiO_2 (100 nm) substrates and identified bilayer lobe areas with different colorations. We have recorded a large number of Raman measurements on different pink-, blue-, and yellow- colored lobe areas; representative zones of measurement are shown in Fig. 1 marked by pink, blue, and yellow circles, respectively. This allowed us to probe twisted bilayer samples with rotation angles from 9° to 16° using Raman spectroscopy.

A detailed inspection of our Raman data from these bilayer zones confirms variations of rotational angles, since different frequencies between 1450 cm^{-1} and 1525 cm^{-1} were found for the R bands, as previously reported elsewhere [18–20].

However, we observed additional peaks at frequencies between 100 and 900 cm^{-1}. Figure 2 shows representative spectra of the samples, where the peaks originating from tBLG are highlighted in yellow and marked with *. We also noticed that the positions of these features are correlated to the previously reported

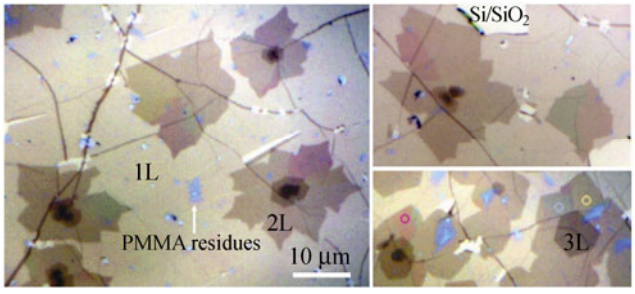

Figure 1 Representative optical micrographs of the studied sample transferred onto a Si/SiO_2 (100 nm) substrate (contrast enhanced), pink-, blue-, and yellow- colored areas can be evidenced in bilayer graphene. Labels identify monolayer (1L), bilayer (2L), and trilayer (3L) areas as well as poly(methyl methacrylate) (PMMA) residues and Si/SiO_2. Pink, blue, and yellow circles exemplify areas where the Raman measurements were recorded.

peak in the vicinity of the G band, assigned to a superlattice-induced Raman process referred as an R band [19]. For all measurements, we used at least two out of the three available laser excitation energies (E_{laser}) noticing that, different from the broadly studied DR Raman effect in graphene-based materials, their frequencies are independent of E_{laser}.

In Fig. 2, the spectra are displayed according to the R frequency evolution; the correlation between the frequencies of the new families of Raman peaks highlighted in yellow and that of the R band is evident. All spectra were taken under resonance conditions by matching E_{laser} with the energy interval between van Hove singularities in the electronic density of states, as reported in Refs. [22, 23].

The origin of the new families of Raman peaks observed in our measurements is elucidated in the plots of Fig. 3. In panel (a), the frequencies of all peaks in Fig. 2, highlighted in yellow marked by *, are plotted as a function of the R peak frequencies, which have been assigned as coming from the in-plane transverse optical (TO) phonon branch [19, 20]. The correlation between the * peak frequencies is obvious, although different trends are observed for distinct families of peaks. Following the assumption that these new features originate from other phonon branches, we have included the theoretical dispersion curves for the ZA, TA, LA, ZO, TO, and LO branches [solid lines in Fig. 3(a)], as a function of the theoretical TO frequency (according to the literature nomenclature: Z stands for out-of-plane modes; T and L stand for

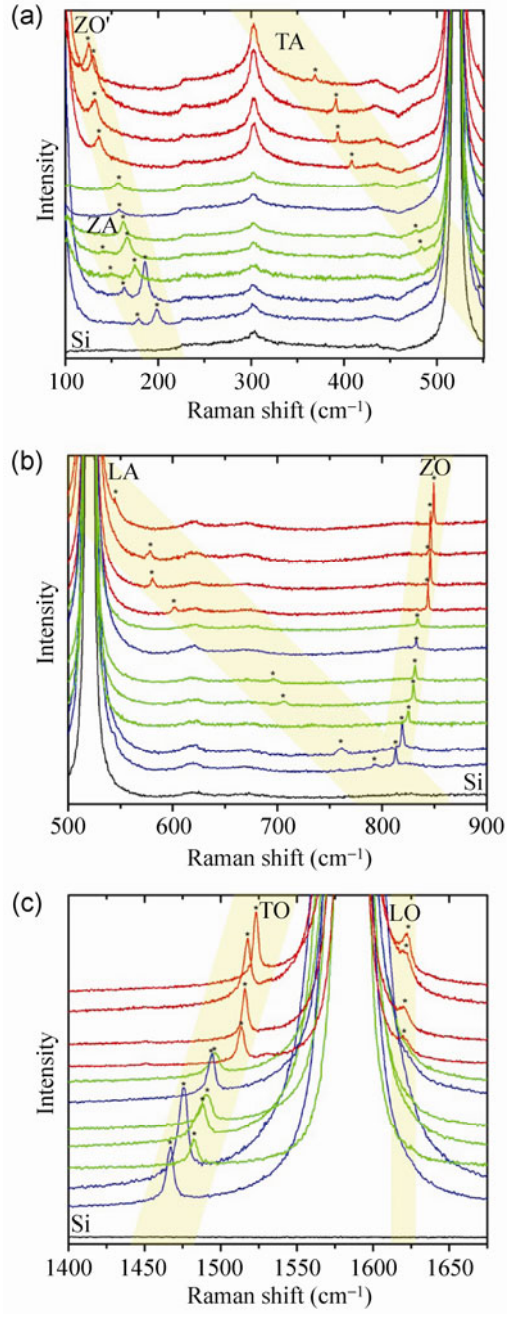

Figure 2 Raman spectra of chemical vapor deposition (CVD)-grown tBLG with different θ values on Si/SiO_2 substrates. (a) 100–550 cm^{-1} range: Three families of new peaks can be observed (highlighted in yellow); (b) 500–900 cm^{-1} range: Two new families of peaks (highlighted in yellow) can be observed; and (c) G band range where the R (transverse optical, TO) and R′ (longitudinal optical, LO) bands are highlighted in yellow. Labels in the yellow areas correspond to the respective phonon branches assigned further in the text and * point to the Raman peaks considered in the study. Curve coloring corresponds to E_{laser} used; red: E_{laser} = 1.96 eV, green: E_{laser} = 2.41 eV and blue: E_{laser} = 2.54 eV, except for the bottom (black) spectra (E_{laser} = 2.41 eV), which correspond to the Si substrate reference signal.

transverse and longitudinal at the zone center Γ, respectively; A and O stand for acoustic and optical, respectively). For that purpose, we have used the phonon dispersion curves calculated by Venezuela et al. [26], along the Γ–K direction (K stands for the Dirac point) in the first Brillouin zone. The actual phonon dispersion curves along the Γ–K direction are depicted in Fig. 3(b), and we have applied an up-shift of 14 cm^{-1} at the TO and LO frequencies to force the matching of the G band frequency at the Γ point (≈ 1585 cm^{-1}). The assignment in Fig. 3(a) clearly shows that, while the R and R′ bands (see Fig. 2) come from the TO and LO phonon branches, respectively, as proposed before [19], most of the additional families of peaks come from other phonon branches predicted theoretically for monolayer graphene.

However, the experimental data marked by open squares clearly deviate from the ZA graphene phonon branch and, as we will discuss later, they are related to the layer breathing vibrations, named ZO′ phonons in AB stacked graphite.

As discussed by Carozo et al. [19], the R band frequency is related to a Raman process which involves the scattering of a photo-excited electron by a phonon with wavevector $\boldsymbol{q}$, and momentum conservation is achieved by the electron being elastically scattered by a superlattice wavevector $-\boldsymbol{q}$ determined by the rotational angle θ. Within the assumption that all other features present in the same spectrum originate from similar processes, and are thereby related to phonons with equal wavevector $\boldsymbol{q}$, we performed the assignment of the experimental data depicted in Fig. 3(a) in the phonon dispersion curves of monolayer graphene shown in Fig. 3(b). First, we assigned the R band frequency observed in the Raman spectrum of each specific sample to the theoretical TO phonon branch, and thus obtained the respective wavevector $\boldsymbol{q}$. Then, we considered the same wavevector to assign all other features observed in the same spectrum. The result is depicted in Fig. 3(b), which shows measured frequencies (solid circles and open squares) as a function of $\boldsymbol{q}$. The assignment of the experimental data to the phonon dispersion curves of monolayer graphene works well for most of the observed families of peaks, except for a low frequency family highlighted

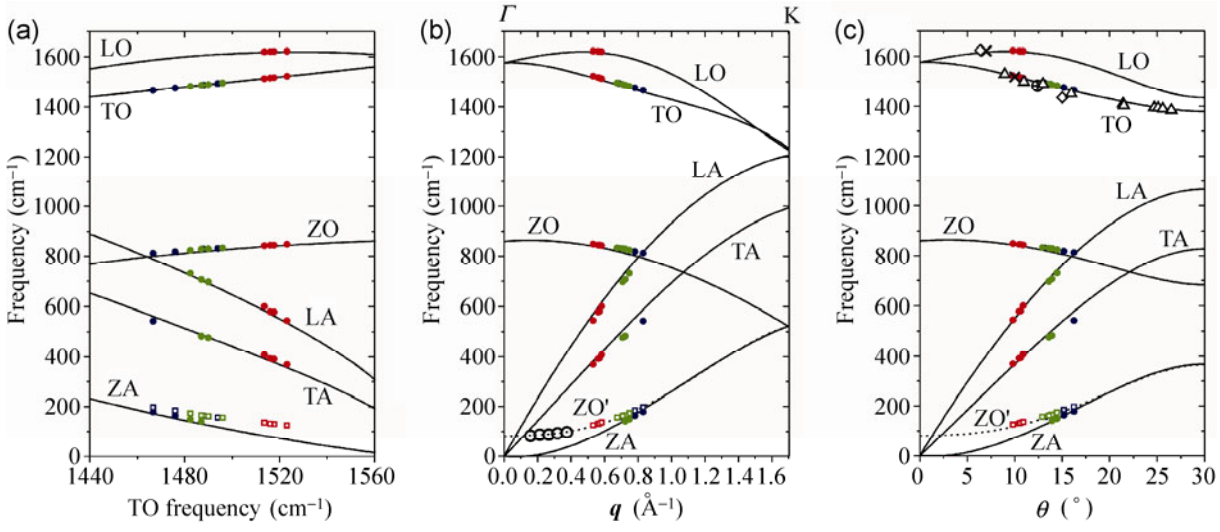

Figure 3 (a) Points indicate Raman frequencies of all the observed families of peaks from Fig. 2 as a function of R band frequencies. Lines stand for the phonon frequencies (branch assignment near each curve) as a function of the TO phonon frequency along Γ–K, as obtained by Venezuela et al. [26]. Red, green and blue symbols stand for measurements obtained with E_{laser} = 1.96, 2.41, and 2.54 eV, respectively. (b) Similar plot as in (a), but with frequencies plotted as a function of the wavevector $\boldsymbol{q}$. The larger open black circles are data from Ref. [27]. (c) In this graph, the wavevectors $\boldsymbol{q}$ from the plot in (b) are replaced by the mismatch angles θ using Eq. (1). The ◊, ×, ⊕, and △ symbols are experimental data obtained from Refs. [19, 22, 23, 28], respectively.

by different symbols (open squares). The origin of these low frequency peaks can be explained by considering layer-breathing mode vibrations (namely the ZO′ mode) occurring in bilayer graphene, multilayer graphene, and graphite. The overtone 2ZO′ has been recently observed for few-layer graphenes (from two to six layers) and graphite [27]. The open black circles in Fig. 3(b) show experimental ZO′ frequencies obtained for bilayer graphene [27], where distinct data points were taken using different laser energies, and the assignment between E_{laser} and $\boldsymbol{q}$ was based on the selection rule for achievement of usual DR condition [4, 5]. Notice that these data points follow the same trend as our experimental data (open squares), and the dashed line in Fig. 3(b) is a tentative dispersion curve for the ZO′ branch in tBLG graphene (along the Γ–K direction) that fits both datasets. The observation of the ZO′ phonon mode in tBLG graphene reveals the interaction between the two rotationally-stacked planes.

According to the superlattice-induced Raman model applied to tBLG described in Ref. [19], the $\boldsymbol{q}$ vector of the phonon involved in the scattering process is related to the rotational angle θ as

$$\boldsymbol{q} = \frac{2\pi}{\sqrt{3}a}\{[-(1-\cos\theta)-\sqrt{3}\sin\theta]\hat{k}_x + [-\sqrt{3}(1-\cos\theta)+\sin\theta]\hat{k}_y\} \quad (1)$$

where a = 2.46 Å is the lattice parameter of graphene, and $\hat{k}_x$ and $\hat{k}_y$ are unit wavevectors, as defined in Fig. 4.

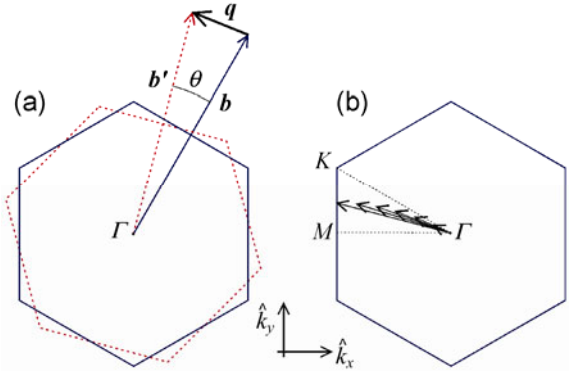

Figure 4 (a) Schematic diagram defining the wavevector $\boldsymbol{q}$ of the superlattice formed by a mismatch angle θ between the two layers. As indicated, $\boldsymbol{q} = \boldsymbol{b'} - \boldsymbol{b}$, where $\boldsymbol{b}$ and $\boldsymbol{b'}$ are primitive reciprocal lattice vectors of the top (first Brillouin zone drawn by solid lines) and bottom (first Brillouin zone drawn by dashed lines) layers, respectively. (b) Schematic diagram showing the evolution of some available $\boldsymbol{q}$ wavevectors by varying θ between 0 and 30 degrees.

Using Eq. (1), we were able to assign the frequencies of the observed Raman features to the rotational angle θ, and the results are depicted in Fig. 3(c). Discrete points are experimental Raman data, and solid lines are theoretical curves obtained by assigning the theoretical curves shown in panel (b) to θ using Eq. (1). The ◊, ×, ⊕, and △ symbols are experimental data obtained from Refs. [19, 22, 23, 28], respectively, where θ was independently determined by microscopy methods (high-resolution transmission electron microscopy [22, 23, 28], scanning tunneling microscopy [28] and lattice resolution atomic force microscopy [19]).

3 Conclusions

We have shown that the superlattice-induced Raman scattering allows us to probe the phonon dispersion of twisted bilayer graphene (tBLG). The process is different from the widely studied DR Raman process in graphene-based materials in many ways: (1) the phonon wavevectors $\boldsymbol{q}$ in the interior of the Brillouin zone can be spanned without changing the excitation laser energy, but by changing the twisting angle θ; (2) first-order scattering is activated by the superlattice modulation, without requiring defects to break the $\boldsymbol{q} \cong 0$ selection rule; (3) the peak frequencies are defined by θ, being independent of E_{laser}; (4) $\boldsymbol{q}$ is not limited to wavevectors close to the high symmetry Γ and K points; (5) $\boldsymbol{q}$ is a θ defined wavevector, including its direction, rather than an average of values around the high symmetry Γ and K points (see Fig. 4). The assignment provided here did not consider the details of the $\boldsymbol{q}$-direction selective process. Deeper explorations can provide accurate experimental information for the development of theoretical models for the phonon dispersion in tBLG, including the coupling between layers in this system which has no AB or ABC stacking.

Materials and methods

The studied tBLG graphene samples were produced by CVD at low pressure using methane as carbon source and copper foil as catalyst [29]. Annealing treatment for 30 min was performed on the copper foil at 1000 ˚C under an Ar/H_2 (10%) low flow. The synthesis was carried out at the same temperature by flowing CH_4 into the growth chamber for 40 min. After this time, the system was allowed to cool down, but the gases flux was maintained. In order to transfer the samples to Si/SiO_2 (100 nm-thick oxide) substrates, a standard transfer process was carried out using PMMA as support layer, and iron chloride ($FeCl_3$) to etch the copper. Raman spectroscopy measurements were performed on a LabRam Horiba instrument with excitation laser energies E_{laser} = 2.54, 2.41, and 1.96 eV. A 1800 g/mm grating was used, and the laser power was maintained below 1 mW.

Acknowledgements

J. C. D. is grateful to Fonds de la Recherche Scientifique (FNRS) and Consejo Nacional de Ciencia y Tecnología (CONACyT) for financial support. A. J. and L. G. C. acknowledge financial support from Conselho Nacional de Desenvolvimento Científico e Tecnológico (CNPq) and Fundação de Amparo à Pesquisa do Estado de Minas Gerais (FAPEMIG).

References

[1] Reich, S.; Thomsen, C.; Maultzsch, J. *Carbon Nanotubes: Physical Concepts and Physical Properties*; Wiley-VCH: Weinheim, 2004.

[2] Saito, R.; Hofmann, M.; Dresselhaus, G.; Jorio, A.; Dresselhaus, M. S. Raman spectroscopy of graphene and carbon nanotubes. *Adv. Phys.* **2011**, *60*, 413–550.

[3] Jorio, A.; Dresselhaus, M. S.; Saito, R.; Dresselhaus, G. *Raman Spectroscopy in Graphene Related Systems*; Wiley-VCH: Weinheim, 2011.

[4] Thomsen, C.; Reich, S. Double resonant Raman scattering in graphite. *Phys. Rev. Lett.* **2000**, *85*, 5214–5217.

[5] Saito, R.; Jorio, A.; Souza Filho, A. G.; Dresselhaus, G.; Dresselhaus, M. S.; Pimenta, M. A. Probing phonon dispersion relations of graphite by double resonance Raman scattering. *Phys. Rev. Lett.* **2002**, *88*, 027401.

[6] Cançado, L. G.; Pimenta, M. A.; Neves, B. R. A.; Dantas, M. S. S.; Jorio, A. Influence of the atomic structure on the Raman spectra of graphite edges. *Phys. Rev. Lett.* **2004**, *93*, 247401.

[7] Maultzsch, J.; Reich, S.; Thomsen, C. Double-resonant Raman scattering in graphite: Interference effects, selection rules, and phonon dispersion. *Phys. Rev. B* **2004**, *70*, 155403.

[8] Cançado, L. G.; Pimenta, M. A.; Saito, R.; Jorio, A.; Ladeira, L. O.; Grueneis, A.; Souza Filho, A. G.; Dresselhaus, G.; Dresselhaus, M. S. Stokes and anti-Stokes double resonance Raman scattering in two-dimensional graphite. *Phys. Rev. B* **2002**, *66*, 035415.

[9] Tan, P. H.; Hu, C. Y.; Dong, J.; Shen, W. C.; Zhang, B. F. Polarization properties, high-order Raman spectra, and frequency asymmetry between Stokes and anti-Stokes scattering of Raman modes in a graphite whisker. *Phys. Rev. B* **2001**, *64*, 214301.

[10] Fantini, C.; Jorio, A.; Souza, M.; Ladeira, L. O.; Souza, A. G.; Saito, R.; Samsonidze, Ge. G.; Dresselhaus, G.; Dresselhaus, M. S.; Pimenta, M. A. One-dimensional character of combination modes in the resonance Raman scattering of carbon nanotubes. *Phys. Rev. Lett.* **2004**, *93*, 087401.

[11] Kürti, J.; Zólyomi, V.; Grüneis, A.; Kuzmany, H. Double resonant Raman phenomena enhanced by van Hove singularities in single-wall carbon nanotubes. *Phys. Rev. B* **2002**, *65*, 165433.

[12] Souza Filho, A. G.; Jorio, A.; Swan, A. K.; Ünlü, M. S.; Goldberg, B. B.; Saito, R.; Hafner, J. H.; Lieber, C. M.; Pimenta, M. A.; Dresselhaus, G. et al. Anomalous two-peak G′-band Raman effect in one isolated single-wall carbon nanotube. *Phys. Rev. B* **2002**, *65*, 085417.

[13] Samsonidze, Ge. G.; Saito, R.; Jorio, A.; Souza Filho, A. G.; Grüneis, A.; Pimenta, M. A.; Dresselhaus, G.; Dresselhaus, M. S. Phonon trigonal warping effect in graphite and carbon nanotubes. *Phys. Rev. Lett.* **2003**, *90*, 027403.

[14] Ferrari, A. C.; Meyer, J. C.; Scardaci, V.; Casiraghi, C.; Lazzeri, M.; Mauri, F.; Piscanec, S.; Jiang, D.; Novoselov, K. S.; Roth, S. et al. Raman spectrum of graphene and graphene layers. *Phys. Rev. Lett.* **2006**, *97*, 187401.

[15] Mafra, D. L.; Samsonidze, Ge. G.; Malard, L. M.; Elias, D. C.; Brant, J. C.; Plentz, F.; Alves, E. S.; Pimenta, M. A. Determination of LA and TO phonon dispersion relations of graphene near the Dirac point by double resonance Raman scattering. *Phys. Rev. B* **2007**, *76*, 233407.

[16] Tuinstra, F.; Koenig, J. L. Characterization of graphite fiber surfaces with Raman spectroscopy. *J. Compos. Mater.* **1970**, *4*, 492–499.

[17] Ferrari, A. C.; Robertson, J. Interpretation of Raman spectra of disordered and amorphous carbon. *Phys. Rev. B* **2000**, *61*, 14095–14107.

[18] Gupta, A. K.; Tang, Y. J.; Crespi, V. H.; Eklund, P. C. Nondispersive Raman D band activated by well-ordered interlayer interactions in rotationally stacked bilayer graphene. *Phys. Rev. B* **2010**, *82*, 241406.

[19] Carozo, V.; Almedia, C. M.; Ferreira, E. H. M.; Cançado, L. G.; Achete, C. A.; Jorio, A. Raman signature of graphene superlattices. *Nano Lett.* **2011**, *11*, 4527–4534.

[20] Righi, A.; Costa, S. D.; Chacham, H.; Fantini, C.; Venezuela, P.; Magnuson, C.; Colombo, L.; Bacsa, W. S.; Ruoff, R. S.; Pimenta, M. A. Graphene Moiré patterns observed by umklapp double-resonance Raman scattering. *Phys. Rev. B* **2011**, *84*, 241409.

[21] Rao, R.; Podila, R.; Tsuchikawa, R.; Katoch, J.; Tishler, D.; Rao, A. M.; Ishigami, M. Effect of layer stacking on the combination Raman modes in graphene. *ACS Nano* **2011**, *5*, 1594–1599.

[22] Kim, K.; Coh, S.; Tan, L. Z.; Regan, W.; Yuk, J. M.; Chatterjee, E.; Crommie, M. F.; Cohen, M. L.; Louie, S. G.; Zettl, A. Raman spectroscopy study of rotated double-layer graphene: Misorientation-angle dependence of electronic structure. *Phys. Rev. Lett.* **2012**, *108*, 246103.

[23] Havener, R. W.; Zhuang, H. L.; Brown, L.; Hennig, R. G.; Park, J. Angle-resolved Raman imaging of interlayer rotations and interactions in twisted bilayer graphene. *Nano Lett.* **2012**, *12*, 3162–3167.

[24] Campos-Delgado, J.; Algara-Siller, G.; Santos, C. N.; Kaiser, U.; Raskin, J. P. Twisted bi-layer graphene: Microscopic rainbows. *Small* **2013**, in press.

[25] Robinson, J. T.; Schmucker, S. W.; Diaconescu, C. B.; Long, J. P.; Culbertson, J. C.; Ohta, T.; Friedman, A. L.; Beechem, T. E. Electronic hybridization of large-area stacked graphene films. *ACS Nano* **2013**, *7*, 637–644.

[26] Venezuela, P.; Lazzeri, M.; Mauri, F. Theory of double-resonant Raman spectra in graphene: Intensity and line shape of defect-induced and two phonon bands. *Phys. Rev. B* **2011**, *84*, 035433.

[27] Lui, C. H.; Malard, L. M.; Kim, S.; Lantz, G.; Leverge, F. E.; Saito, R.; Heinz, T. F. Observation of layer-breathing mode vibrations in few-layer graphene through combination Raman scattering. *Nano Lett.* **2012**, *12*, 5539–5544.

[28] Wang, Y. N.; Su, Z. H.; Wu, W.; Nie, S.; Xie, N.; Gong, H. Q.; Guo, Y.; Lee, J. H.; Xing, S. R.; Lu, X. X. et al. Twisted bilayer graphene superlattices. *arXiv*, in press, DOI: arXiv:1301.4488. http://arxiv.org/abs/1301.4488.

[29] Li, X. S.; Cai, W. W.; An, J. H.; Kim, S.; Nah, J.; Yang, D. X.; Piner, R.; Velamakanni, A.; Jung, I.; Tutuc, E. et al. Large-area synthesis of high-quality and uniform graphene films on copper foils. *Science* **2009**, *324*, 1312–1314.